A Foward-Swept-Wing Fighter Configuration Designed by a Transonic Computational Method

Michael J. Mann* and Charles E. Mercer†
NASA Langley Research Center, Hampton, Virginia

Supercritical technology has been applied to the design of a forward-swept wing fighter configuration and an assessment has been made of the relative performance of forward vs aft sweep. The wing and canard for this forward-swept wing configuration were designed for transonic manuever by the use of a transonic computational analysis method and a transonic design procedure. A model of this configuration and was tested in the Langley 16-ft Transonic Tunnel. The transonic theory gave a reasonably good estimate of the wing pressure distributions at transonic maneuver conditions. Comparison of this configuration with an equivalent aft-swept wing configuration showed that, at a Mach number of 0.9 and a life coefficient of 0.9, the two configurations have the same trimmed drag. This forward-swept wing configuration was also found to have good maneuver performance relative to the Rockwell International HiMAT highly maneuverable aircraft configuration.

Nomenclature

Wing geometric parameters A, $\bar{c}$, S, and λ are for basic trapezoidal wing extended to the model centerline.

A = aspect ratio
b = wing span
C_D = drag coefficient
C_{D_0} = zero lift turbulent skin-friction drag coefficient
C_L = total lift coefficient
$C_{L,\text{th}}$ = theoretical lift coefficient of wing and canard (if present) in the presence of an infinite cylinder
C_m = pitching moment coefficient (referred to a moment center 23.9 in. from fuselage nose for forward-swept wing)
C_p = pressure coefficient
c = local wing chord, parallel to plane of symmetry
$\bar{c}$ = wing mean aerodynamic chord
D = drag
L = total lift
M = freestream Mach number
q = freestream dynamic pressure
$Re_{\bar{c}}$ = Reynolds number based on $\bar{c}$
S = wing reference area
$S_{c,\text{exp}}$ = exposed canard area
$S_{t,\text{exp}}$ = exposed horizontal tail area
t/c = ratio of maximum section thickness at a given span station to the local wing chord parallel to plane of symmetry
x = local chordwise distance from wing leading edge, parallel to plane of symmetry
x_{cg} = center of gravity (moment reference) measured from fuselage nose
Y = spanwise distance from plane of symmetry
α = angle of attack
α' = α + const, where constant is selected to make $\alpha' = 0$ when $C_L = 0$
δ_c = canard deflection, positive leading edge up
$\delta_{f,\text{LE}}$ = leading-edge flap deflection, positive with leading edge down
$\delta_{f,\text{TE}}$ = trailing-edge flap deflection, positive with trailing edge down
δ_t = horizontal tail deflection, positive with leading edge up
$\Delta C_{p_{\text{sh}}}$ = change in C_p across shock wave
η = semispan location, $y/(b/2)$
λ = taper ratio

Presented as Paper 85-4069 at the AIAA 3rd Applied Aerodynamics Conference, Colorado Springs, CO, Oct. 14-16, 1985; received Nov. 17, 1985; revision received March 12, 1986.

*Aerospace Engineer. Member AIAA.
†Aerospace Engineer.

Introduction

RECENT developments in composite structures have opened the possibility of forward-swept wings that exhibit good static divergence characteristics with acceptable levels of structural mass.[1,2] These developments have led to several studies of the application of forward sweep to highly maneuverable aircraft.[3-11] At maneuver conditions, the flow on a forward-swept wing generally separates first in the root region. At transonic speeds, this separation is induced by the development of a strong inboard shock wave and, possibly, the simultaneous presence of a strong adverse pressure gradient. This provides the opportunity to include on the aircraft some aerodynamic device that will have a strong favorable interference effect on the region of the wing where the flow first separates. For example, a canard with positive lift induces a downwash on the wing root, lowering the local angle of attack on that part of the wing. If the wing is designed to operate in the presence of this canard-induced flowfield, this lower local angle of attack will reduce the flow separation and, therefore, the drag. Forebody strakes can also be utilized to provide favorable effects on a forward-swept wing.[11,12]

Since the flow on an aft-swept wing generally separates first at the wing tip, the favorable interference effects of a canard are not quite so clear as in the case of a forward-swept wing. The downwash from the canard unloads the wing root, which, in turn, produces less upwash at the wingtip. However, the canard itself produces an upwash at the wing tip, which tends to increase the local angle of attack in that region.

Recent studies have examined the application of supercritical technology to the improved maneuver performance of wings with moderately swept-back leading edges.[13] The purpose of the present investigation has been to study the application of supercritical technology to a forward-swept wing fighter configuration and to make some assessment of the relative performance of forward vs aft sweep. The wing and canard for this forward-swept wing configuration were designed for transonic maneuver by the use of a transonic

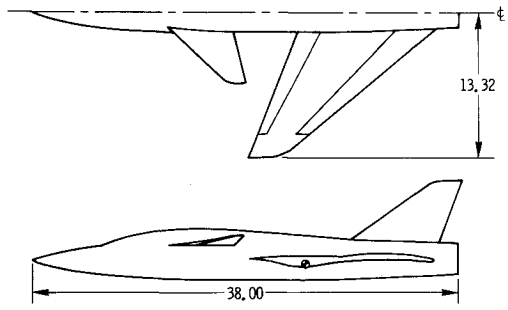

Fig. 1 General arrangement of model (dimensions in inches).

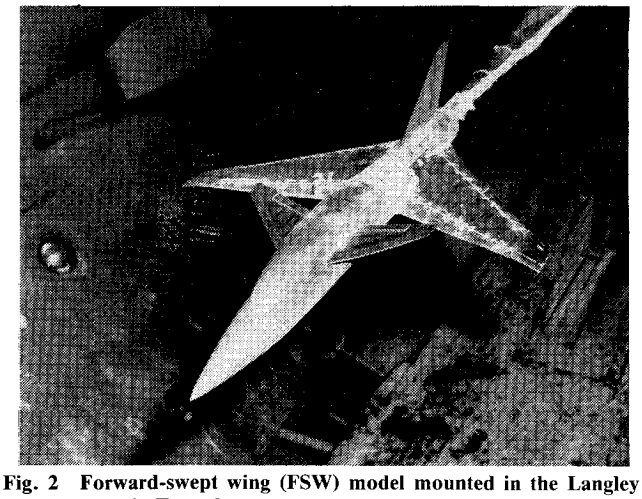

Fig. 2 Forward-swept wing (FSW) model mounted in the Langley 16-ft Transonic Tunnel.

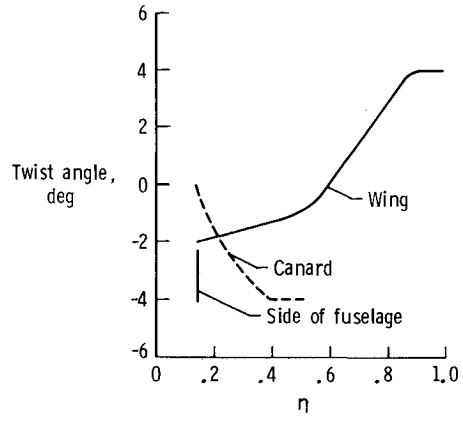

Fig. 3 Twist distribution for wing and canard of FSW model.

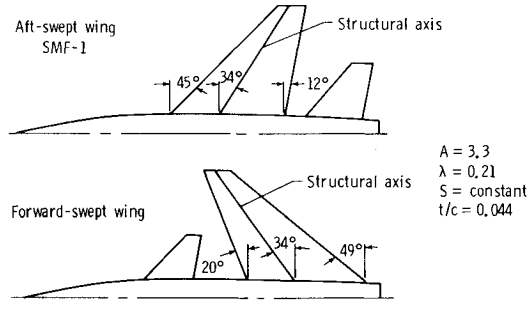

Fig. 4 Geometry of forward-swept and SMF-1 aft-swept wings.

computational analysis method and a transonic design procedure. The computational method calculates the transonic flow over a canard/wing/fuselage combination so that the strong transonic induced-flow effects of the canard on the wing are taken into account.

A model of this forward-swept wing configuration was tested in the Langley 16-ft Transonic Tunnel. The wing pressure distributions were measured and have been compared with the theoretical calculations. The lift and drag characteristics have been compared with an equivalent aft-swept wing configuration and with the HiMAT highly maneuverable aircraft configuration.

Transonic Maneuver Configurations

Forward-Swept Wing

The wind tunnel model is shown in Figs. 1 and 2. The model represents a highly maneuverable fighter configuration equipped with a forward-swept wing and with a canard for pitch control. The incidence of the canard can be varied and the wing leading- and trailing-edge flaps can be deflected.[14]

The fuselage was area ruled by the use of the supersonic design and analysis method of Ref. 15. The area distribution was designed to reduce the zero lift wave drag, subject to certain requirements. In addition to the usual requirement of sufficient internal volume for instrumentation, the fuselage was required to have a flat side on the canopy to allow for canard rotation and smooth streamwise contour lines. The wave drag was examined for Mach numbers betwen 1.0 and 1.6. The supersonic code was also used to define the negative trailing-edge flap deflection angle necessary for low drag at a Mach number of 1.2. The model does not have a flow-through nacelle.

The wing and canard twist distributions are shown in Fig. 3. The vortex lattice design method of Ref. 16 was used to calculate the twist of the wing in the presence of the canard. The wing twist shown in Fig. 3 is a compromise between the optimum twist distributions for transonic maneuver and cruise. The canard has the same planform as the transonic wing design of Ref. 13. Therefore, the twist of that wing was reduced slightly to allow for the cruise requirements and was then utilized as the canard twist for the present study.

In order to make some assessment of the relative performance of forward vs aft sweep, the planform of the swept-forward wing was designed as a counterpart of the planform for the SMF-1 aft-swept wing described in Ref. 13. As shown in Fig. 4, the wings for these configurations have the same aspect ratio, taper ratio, and wing area. The structural axes for these wings have been assumed to lie along the 40% chord line. The sweep of the 40% chord line on the forward-swept wing is the negative of the sweep back of the 40% chord line on the aft-swept wing. This would make the structural weights of these wings approximately the same on an actual aircraft.

The section shapes of both the forward-swept wing and the SMF-1 aft-swept wing have been designed for good transonic maneuver performance through the use of current transonic computational methods and the supercritical technology development discussed in Ref. 13. The forward-swept wing was designed for a Mach range of 0.85-0.95 and a lift coefficient of 0.9. The SMF-1 was designed for a Mach number of 0.9 and a lift coefficient of 0.9. Table 1 compares the areas of the canard and the horizontal tail for these configurations. The transonic maneuver performance of these configurations will be compared.

The canard planform of the forward-swept wing configuration was chosen to be aft swept because this would seem to have a more favorable influence on the wing than a forward-swept canard. The flow on the swept-forward wing separates first at the root and the flow on the swept-back canard separates first at the tip. Therefore, the downwash from the root region of the canard, where the flow remains attached at maneuver conditions, helps to reduce the flow separation in the root region of the wing.

Table 1 Comparison of configurations[a]

Configuration	A	λ	$S_{c,exp}/S$	$S_{t,exp}/S$
FSW	3.28	0.2142	0.156	—
SMF-1	3.28	0.2142	—	0.245
HiMAT	3.85	0.25	0.301	—

[a]All wing quantities refer to basic trapezoidal wing extended to the model centerline.

The forward-swept wing model was tested in the Langley 16-ft Transonic Tunnel. The tests were run at Mach numbers of 0.60-1.2 and angles of attack between −4 and 17 deg. The Reynolds number, based on wing mean aerodynamic chord, varied from 2.5×10^6 at Mach 0.60 to 3.0×10^6 at Mach 1.2.

Aerodynamic forces and moments were measured by an internal, six-component, strain gage balance. The angle of attack was corrected for flow angularity. Boundary-layer transition strips were applied to the wings, canard, vertical tail, and fuselage nose using the method of Ref. 17. The wing was instrumented with flush surface, static pressure orifices.

Comparison Configuration

The maneuver performance of the forward-swept wing configuration is also evaluated by comparison with the HiMAT highly maneuverable aircraft configuration. The HiMAT is a recently developed configuration[18] for which supercritical technology has been utilized to achieve good transonic maneuver performance at a Mach number of 0.9 and a lift coefficient of about 1.0. Some parameters for the HiMAT are also given in Table 1 and a sketch of the model is shown in Fig. 5.

Computational Method and Design Considerations

The airfoil sections of the forward-swept wing were designed in the presence of the canard. The configuration was designed for a maneuver lift coefficient of 0.9 over the Mach range of 0.85-0.95. The thin supercritical sections for the wing and the canard were designed by the use of a three-dimensional transonic computational analysis method and a transonic design procedure. The transonic computational analysis method used is called PANDORA.[19] The PANDORA computer code was selected because it calculates the transonic flow over a canard/wing/fuselage configuration and, therefore, accounts for the strong transonic induced-flow effects of the canard on the wing.

Although the PANDORA code was used strictly as a transonic analysis method in the current study, the PANDORA code can also be utilized as an automated design tool through the combined use of the transonic analysis method and numerical optimization. In the present study, however, an alternate design procedure was chosen that, it was felt, would result in a much more direct method of achieving the desired type of wing pressure distributions at the selected maneuver design conditions. The transonic design procedure described in Refs. 20 and 21 was utilized along with the PANDORA transonic analysis method for the wing and canard design. This design procedure provides a set of guidelines for the systematic alteration of wing shape to achieve some desired pressure distribution.

Since the forward-swept wing configuration was designed, additional developments in transonic design methods have taken place (see, for example, Refs. 22-24). The recently developed method of Ref. 24 is an improved version of PANDORA (called TRO-3D). In this new method, the optimization process has been tailored to transonic aerodynamic design so that better designs should result (more reliable optimums) and the computational run times should be greatly reduced.

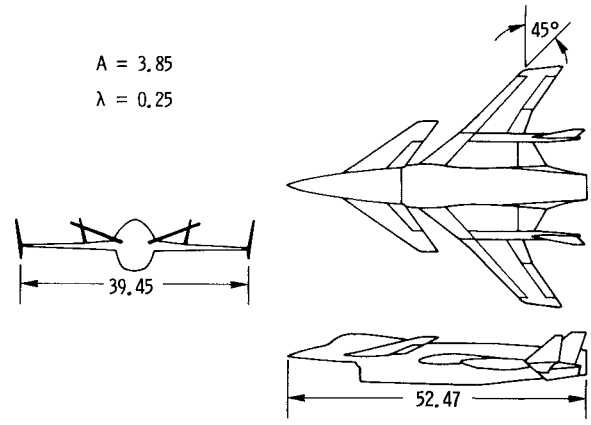

Fig. 5 HiMAT configuration (dimensions in inches).

The flow equation used in the analysis by the PANDORA code[19,24] is an "extended" transonic small-disturbance equation. It is solved by the use of finite difference approximations in a global crude Cartesian mesh system with individual embedded fine grids placed over the wing and the canard. The crude grid has 64 streamwise, 26 spanwise, and 31 vertical grid points. The fine grid is in vertical planes with 133 streamwise and 25 vertical grid points. There are 15 fine grid planes across the wing semispan and 8 planes on the canard semispan. The fine grid density is reduced at the wing and canard tips. The effects of viscosity are included by the use of a modified two-dimensional Bradshaw turbulent-layer analysis and infinite swept-wing theory. For the maneuver conditions calculated in this study, the solution was found to be essentially converged with 100 crude grid iterations followed by 160 crude/fine grid iterations. The boundary-layer solution was updated every 20 iterations during the crude/fine grid calculations.

The initial efforts of this study were to design a configuration with a forward-swept wing but without a canard. The results of these initial efforts indicated that, based on the studies of Ref. 13, the inboard flow would experience extensive separation due to the presence of a strong inboard shock wave preceded by a strong adverse pressure gradient. Therefore, a canard was added to the configuration and the wing sections were redesigned in the presence of the canard. Based on these theoretical results and the studies of Ref. 13, it was felt that the wing would develop less flow separation for the case of the canard configuration than for the case of the configuration designed without a canard.

The objective of the design process was to reduce the shock strength and the adverse pressure gradients at a lift coefficient of 0.9 over the Mach range of 0.85-0.95. The studies of Ref. 13 on the maneuver performance of aft-swept wings (without canards) indicated that it was desirable to design the wing so that, at a Mach number of 0.9, the upper surface pressure distribution was somewhat flattened on the forward part of the wing. Therefore, an effort was made to design the forward-swept wing with this type of pressure distribution on the outboard part of the wing at a Mach number of 0.9 and a lift coefficient of 0.9. The inboard part of the wing was designed to eliminate the strong shocks preceded by strong adverse pressure gradients. The resultant inboard flow tends to have moderately strong shocks preceded by a favorable pressure gradient (see Fig. 6). These inboard pressure distributions are not necessarily optimum; however, they appeared to be a significant improvement over the canard-off case. Oil flow studies showed that, for example, at Mach 0.85 and 0.88 lift coefficient, the flow on the wing in the presence of the canard is predominantly attached with a small region of separation at the trailing edge.

Since the canard has the same planform as the SMF-1 wing, the midspan airfoil section of SMF-1 was somewhat modified and used on the canard. The modifications resulted

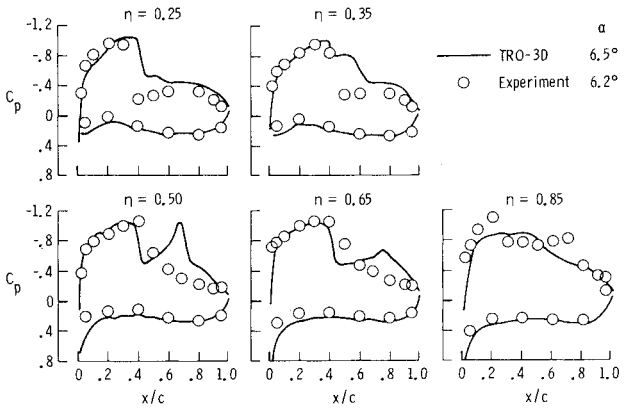

a) $M=0.85$, $C_L=0.83$.

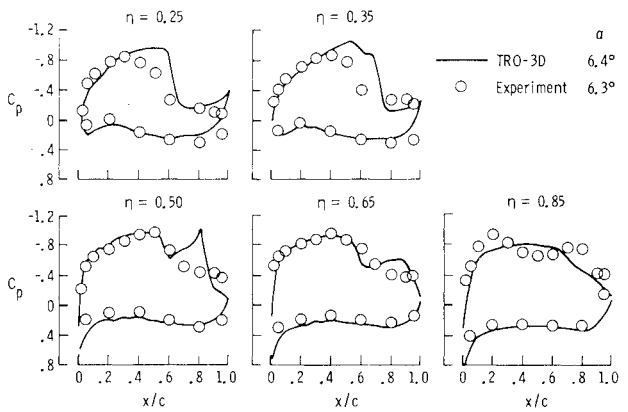

b) $M=0.90$, $C_L=0.85$.

Fig. 6 Comparison of theoretical and experimental wing pressure distributions for FSW configuration: $\delta_c=0$, $\delta_{f,LE}=\delta_{f,TE}=0$.

in two new sections, one for the root and one for the tip. Only two sections were defined in order to simplify the model construction process.

Figure 6 shows a correlation between the theoretical wing pressure distributions of PANDORA and the experimental pressure distributions. Results are shown for Mach numbers of 0.85 and 0.9 at lift coefficients of 0.83 and 0.85, respectively. The fuselage was represented in the calculations by an infinite cylinder. The experimental lift coefficients selected were approximately 0.1 greater than the theoretical lift coefficients. This was done in order to account for the lift on the fuselage, which is not accounted for by PANDORA in the case of an infinite cylinder. The canard incidence and all flap deflection angles are zero.

The correlation for both Mach numbers is good considering the high levels of lift involved. The trailing-edge region of the wing apparently has some separation, as indicated by the lack of good upper surface trailing-edge pressure recovery in the experimental data. This separation would tend to push the trailing-edge shock wave forward and explain the differences in shock location between the theory and the experiment on the inboard region of the wing. The difference in character between the theory and the experiment on the upper surface at $\eta=0.85$ may be caused by the reduction in the number of fine grid points in the theory from 70 over most of the wing to 11 at the wing tip. The upturn in the theoretical pressure at the inboard trailing edge for a Mach number of 0.9 is thought to be caused by some peculiarity in the extrapolation of the boundary layer past the computed separation point.

Evaluation of Forward-Swept-Wing Configuration

Maneuver Efficiency

Figure 7 presents drag polars for the forward-swept wing (FSW) configuration at Mach numbers of 0.60 and 0.9. The

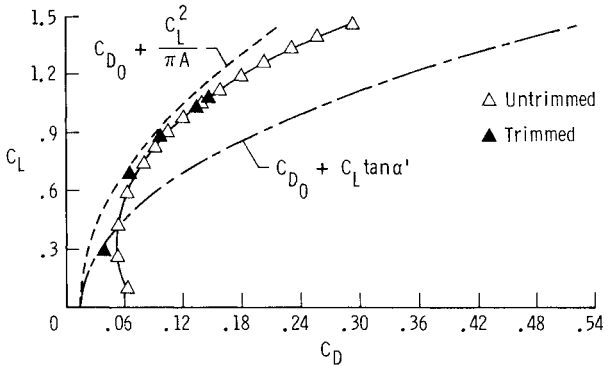

a) $M=0.60$; untrimmed data: $\delta_c=0$, $\delta_{f,TE}=\delta_{f,LE}=10$ deg.

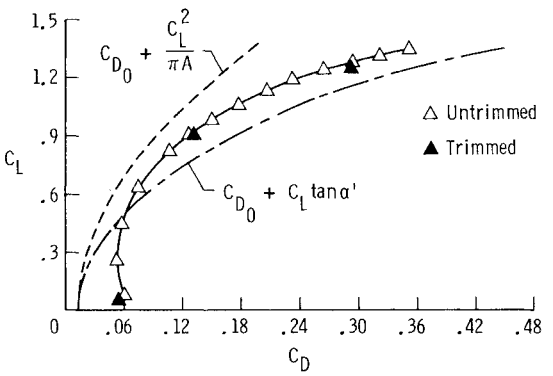

b) $M=0.90$; untrimmed data: $\delta_c=0$, $\delta_{f,TE}=10$ deg, $\delta_{f,LE}=0$.

Fig. 7 Maneuver efficiency for FSW configuration.

available trimmed points are indicated by solid symbols. Since only a few trimmed points are available, Figs. 7a and 7b also show untrimmed data for a configuration with fixed-flap and canard deflections. The chosen flap deflection angles reduce the drag above the design lift condition, while, of course, they increase the drag at the low lift coefficients. Figure 7 also shows the ideal polar corresponding to an elliptic lift distribution (100% suction) and the $C_L\tan\alpha'$ curve corresponding to a zero suction condition of a flat/plate wing. The C_{D_0} is a zero-lift turbulent skin-friction drag coefficient. The skin friction was calculated with the Kármán-Schoenherr formula for incompressible turbulent flow on a flat plate at zero incidence.[25] The skin-friction drag was then corrected for compressibility by the Sommer and Short T' method[26] and corrected for thickness by the method of Hoerner.[27]

At Mach 0.60 and design lift coefficient 0.9, the FSW configuration has achieved most of the available potential for drag reduction based on the limits indicated by the two theoretical curves. However, at Mach 0.9 and the same lift coefficient, the experimental results are only about midway between the theoretical limits. It would appear, therefore, that, although it is not expected that the theoretical minimum of this ideal polar could be exactly achieved, there is some potential for further drag reduction at Mach 0.9 and lift coefficient 0.9. Any transonic maneuver drag reduction must be made, of course, for the entire range of transonic speeds and not just for Mach 0.9. An improved transonic computational design code such as TRO-3D would appear to offer potential for further improvements.

Forward vs Aft Sweep

Figure 8 shows the spanwise variation of theoretical shock strength on the forward-swept wing configuration and its aft-swept counterpart (SMF-1). The pressure increase through the shock wave was computed with the PANDORA code. The fuselage for both configurations was represented by an infinite cylinder. The calculations were made for a

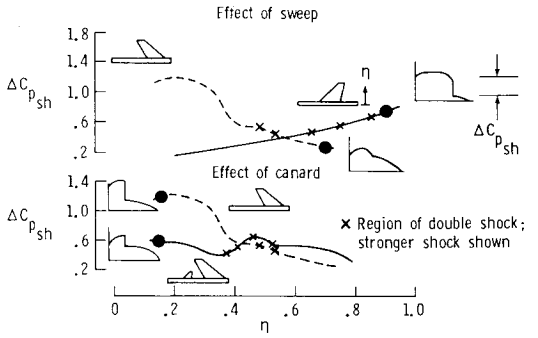

a) $M=0.85$.

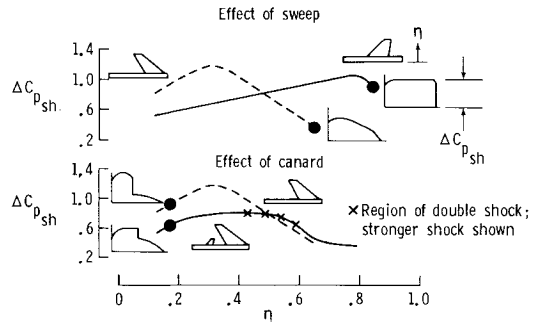

b) $M=0.90$.

Fig. 8 Spanwise variation of theoretical shock strength on forward-swept and SMF-1 aft-swept wings: $\delta_c=0$, $\delta_{f,\mathrm{LE}}=\delta_{f,\mathrm{TE}}=0$, $C_{L,\mathrm{th}}=0.7$.

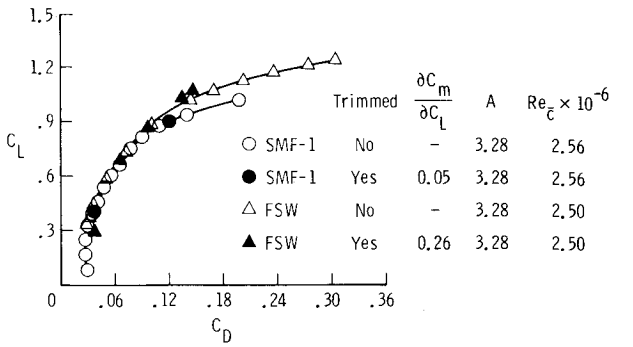

a) $M=0.60$, $x_{cg}=22.4$ in. for SMF-1.

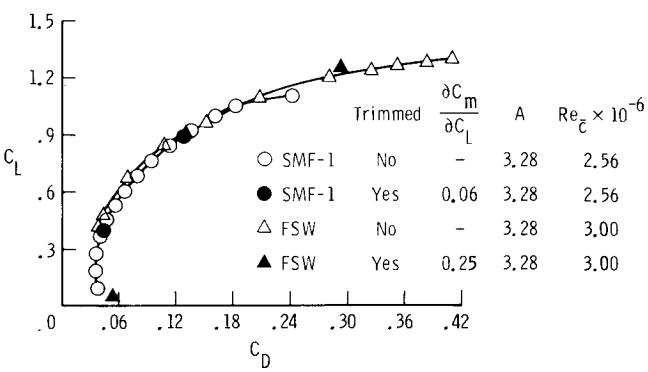

b) $M=0.90$, $x_{cg}=23.0$ in. for SMF-1.

Fig. 9 Comparison of forward-swept and SMF-1 aft-swept wing configurations; untrimmed data: $\delta_t=0$, $\delta_c=0$, $\delta_{f,\mathrm{TE}}=\delta_{f,\mathrm{LE}}=0$.

theoretical lift coefficient (excluding fuselage lift) of 0.7 at Mach 0.85 and 0.9. This theoretical lift coefficient would correspond to a total lift coefficient of about 0.8. In places where a double-shock system exists, the stronger shock jump is plotted. These locations are indicated by an X.

The upper portions of Fig. 8 illustrate one of the fundamental aerodynamic differences between forward and aft sweep. The shock strength is greatest at the tip of the aft-swept wing and greatest at the root of the forward-swept wing.

As mentioned earlier, it was decided to include a canard on the forward-swept wing configuration in order to obtain an inboard chordwise pressure distribution that, it was felt, would result in a reasonably attached flow at transonic maneuver conditions. The lower parts of Fig. 8 show the distribution of shock strength on the current forward-swept wing configuration with and without a canard. The calculations were made at a fixed lift coefficient and the same computational grid was used on the wing for both cases. Of course, these results do not show the differences that would result if one wing were designed without a canard and the other wing were designed in the presence of a canard; however, they do graphically illustrate the powerful influence of the canard on the wing flowfield. They show a considerable reduction in shock strength at the wing root with the canard present. The decrease in shock strength is due to the downwash behind the canard and to the somewhat lower angle of attack necessary to develop the same value of lift (about 1 deg lower). When the effect of the canard is calculated with the angle of attack fixed at the value for the case with the canard on, the decrease in shock strength is on the order of 80-90% of that shown in Fig. 8. This result would indicate that most of the canard effects shown in Fig. 8 are caused by the induced-flow effects from the canard. The addition of the canard also produces a small increase in the strength of the outboard wing shock, apparently due to the upwash induced by the canard outboard of its tip.

The lift and drag characteristics of the forward- and aft-swept configurations are shown in Fig. 9. Results are shown for Mach numbers of 0.60 and 0.90 and the trimmed points are again indicated by solid symbols. The untrimmed data for FSW are for zero flap deflections (SMF-1 does not have leading or trailing-edge flaps). The aspect ratios of the two configurations are the same and the test Reynolds numbers are very close. The locations of the center of gravity for SMF-1 were selected to produce minimum, trimmed drag at cruise and maneuver conditions for the available tail deflection angles (only negative tail settings were tested). The center of gravity chosen for the FSW configuration allowed it to be trimmed,[14] with various flap deflection angles, at angles of attack of 4-22 deg at a Mach number of 0.3. At higher Mach numbers, it was found that small changes from this center of gravity did not have a significant effect on the trimmed drag for a lift coefficient of 0.9. Both configurations are unstable at the chosen center of gravity locations. Their stability levels in terms of $\partial C_m/\partial C_L$ are shown in the legends for Fig. 9 and are reasonable values for their respective configurations.

Both of these configurations were designed for a lift coefficient of 0.9. At Mach 0.9 and a lift coefficient of 0.9, the two configurations have the same trimmed drag. Oil flow photographs of these configurations at a Mach number of 0.90 show that, at a lift coefficient of 0.85, SMF-1 has a small amount of trailing-edge and wing tip separation and that, at a lift coefficient of 0.83, the FSW has some separation in the trailing-edge region. For conditions somewhat above the design lift coefficient, however, the FSW configuration has lower drag than the aft-swept SMF-1, which is probably due to less flow separation on the FSW caused by the favorable influence from the canard. Similar results were obtained at Mach 0.60.

The comparisons of Fig. 9 suggest that additional studies need to be conducted in order to evaluate the influence of the canard on the aft-swept SMF-1 configuration.

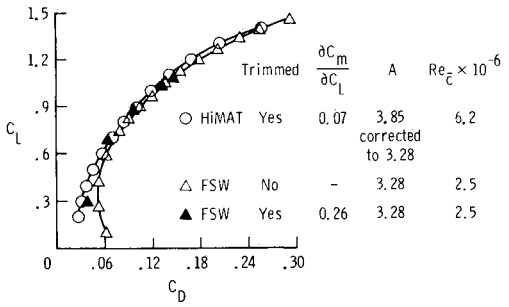

a) $M=0.60$; untrimmed data for FSW: $\delta_c=0$, $\delta_{f,TE}=\delta_{f,LE}=10$ deg; HiMAT maneuver configuration.

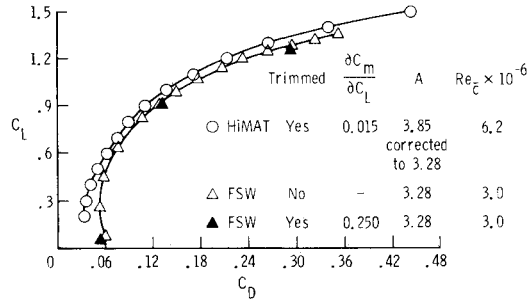

b) $M=0.90$; untrimmed data for FSW: $\delta_c=0$, $\delta_{f,TE}=10$ deg, $\delta_{f,LE}=0$; HiMAT maneuver configuration.

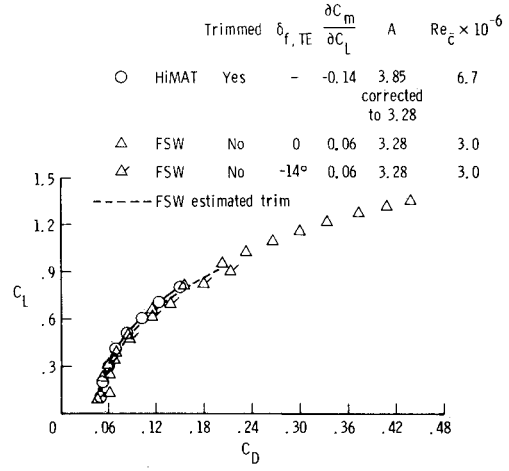

c) $M=1.2$; untrimmed data for FSW: $\delta_c=0$, $\delta_{f,LE}=0$; HiMAT cruise configuration.

Fig. 10 Comparison of forward-swept wing configuration with HiMAT.

Comparisons with HiMAT

The forward-swept wing configuration is further evaluated by comparison with the HiMAT highly maneuverable aircraft configuration. Figure 10 compares the HiMAT and FSW configurations at Mach numbers of 0.60, 0.90, and 1.2. The results for the HiMAT at Mach 0.60 and 0.90 are for the maneuver configuration and the results at Mach 1.2 are for the cruise configuration.[18] The HiMAT data are trimmed and the solid symbols for FSW are trimmed. The untrimmed data for FSW at Mach 0.60 and 0.90 have the same flap deflections as Fig. 7. The untrimmed data for FSW at Mach 1.2 are plotted for two flap deflection angles in order to estimate trimmed conditions. The HiMAT data have been corrected from an aspect ratio of 3.85 to the value of 3.28 for the FSW (assuming an induced-drag correction factor $e=1$). The difference in test Reynolds numbers (see figure legend) for these two configurations was found to change the C_{D_0} of FSW by only 20 counts (0.0020) and is, therefore, not a significant factor in these comparisons. The values of $\partial C_m/\partial C_L$ are again noted in the figures.

Figures 10a and 10b show that, at Mach 0.60 and 0.90, the HiMAT has lower drag than FSW, although the drag levels are reasonably close at maneuver conditions. A Mach number of 0.90 and a lift coefficient of 0.9 approximates the transonic maneuver design point for both configurations. When the actual value of e is used to correct the HiMAT data for the aspect ratio and the effect of the winglets on the HiMAT is accounted for, the trimmed drag at Mach 0.90 and lift coefficient 0.9 is essentially the same for both configurations. The high drag for FSW at the low levels of lift is due to the large amount of camber in the wing. This camber is required for maneuver and could be reduced by means of variable geometry as illustrated in Fig. 10c for $\delta_{f,TE}=-14$ deg. Figure 10c shows that the FSW has comparable performance to the HiMAT at Mach 1.2. At a lift coefficient of 0.082, corresponding to level flight of the HiMAT at 30,000 ft altitude with one-half fuel load, the two configurations appear to have about the same value of trimmed C_D.

Conclusions

This study has examined the application of supercritical technology and a transonic computational analysis method to the design of a forward-swept wing configuration for good transonic maneuver performance. This configuration was equipped with a canard and the induced-flow effects of the canard on the wing were accounted for by the computational method. A transonic design procedure was used to provide a set of guidelines for the iterative application of the computational method during the design process. The results of this study of a forward-swept wing fighter may be summarized as follows:

1) The PANDORA transonic computational method predicted wing pressure distributions that showed reasonably good correlation with experimental results for Mach numbers of 0.85 and 0.90 at lift coefficients of 0.83 and 0.85, respectively.

2) The use of the PANDORA code and the transonic design procedure indicated that, if the forward-swept wing were designed in the presence of the canard, a chordwise pressure distribution could be developed at transonic maneuver conditions which would produce less flow separation than the pressure distribution resulting for a wing designed without the canard. Oil flow photographs at Mach numbers of 0.85 and 0.9 for lift coefficients of 0.88 and 0.83, respectively, indicated that the wing flow was attached except for some separation in the trailing-edge region.

3) Comparison of the drag polar with the ideal polar and the flat-plate wing or zero-suction polar at the design lift coefficient of 0.9 showed that, at Mach 0.60, most of the available potential for drag reduction had been achieved; however, at Mach 0.9 and a lift coefficient of 0.9, there appeared to be some potential for further drag reduction.

4) Comparison of the forward-swept wing configuration with a corresponding aft-swept wing configuration showed that the two configurations had the same trimmed drag at Mach 0.90 and a lift coefficient of 0.9; however, at higher lift coefficients, the forward-swept configuration had lower drag, probably due to the favorable influence of the canard.

5) The forward-swept wing configuration showed good maneuver performance at Mach 0.60, 0.9, and 1.2 relative to the HiMAT advanced technology highly maneuverable fighter configuration. At Mach 0.9 and a lift coefficient of 0.9, which approximates the transonic maneuver design point for both configurations, the trimmed drag was the same for both configurations.

References

[1]Krone, N. J., "Divergence Elimination with Advanced Composites," AIAA Paper 75-1009, Aug. 1975.

[2]Ricketts, R. H. and Doggett, R. V. Jr., "Wind-Tunnel Experiments on Divergence of Forward-Swept Wings," NASA TP-1685, Aug. 1980.

[3]Uhuad, G. C., Weeks, T. M., and Large, R., "Wind Tunnel Investigation of the Transonic Aerodynamic Characteristics of For-

ward Swept Wings," *Journal of Aircraft,* Vol. 20, March 1983, pp. 195-202.

[4]Moore, M. and Frei, D., "X-29 Forward Swept Wing Aerodynamic Overview," AIAA Paper 83-1834, July 1983.

[5]Spacht, G., "The Forward Swept Wing: A Unique Design Challenge," AIAA Paper 80-1885, Aug. 1980.

[6]Miller, B. D. and Hadley, S. K., "Application of Forward Sweep Wings to an Air Combat Fighter," AIAA Paper 83-1833, July 1983.

[7]Hadley, S. K. and Miller, B. D., "Application of Forward Swept Wings to an Air Combat Fighter," AIAA Paper 80-1883, Aug. 1980.

[8]Robinson, M. R. and Robinson, D. A., "Forward Swept Wing (FSW) Designs: A High Payoff Through Technology Integration," AIAA Paper 80-1884, Aug. 1980.

[9]Stanniland, D. R., "Aspects of the Aerodynamic Design of a Thin Supercritical, Forward Swept Wing for a Combat Aircraft," *Proceedings of the International Conference on Forward Swept Wing Aircraft,* Bristol, England, March 1982, pp. I.13.1-I.13.13.

[10]Huffman, J. K. and Fox, C. H. Jr., "Subsonic Longitudinal- and Lateral-Directional Static Aerodynamic Characteristics for a Close-Coupled Wing-Canard Model in Both Swept-Back and Swept-Forward Configurations," NASA TM-74092, 1978.

[11]Huffman, J. K and Fox, C. H. Jr., "Subsonic Longitudinal- and Lateral-Directional Static Aerodynamic Characteristics for a Model with Swept-Back and Swept-Forward Wings," NASA TM-74093, 1978.

[12]Poll, D. I. A. and Qui, C. H., "A Comparison of the Aerodynamic Characteristics of Swept Forward and Swept Back Wings Including the Effect of Strakes," *Proceedings of the International Conference on Forward Swept Wing Aircraft,* Bristol, England, March 1982, pp. I.20.1-I.20.15.

[13]Mann, M. J., Campbell, R. L., and Ferris, J. C., "Aerodynamic Design for Improved Maneuverability by Use of Three-Dimensional Transonic Theory," NASA TP-2282, Feb. 1984.

[14]Gainer, T. G., Mann, M. J., and Huffman, J. K., "Low-Speed Investigation of Effects of Wing Leading- and Trailing-Edge Flap Deflections and Canard Incidence on a Fighter Configuration Equipped with a Forward-Swept Wing," NASA TM-85795, July 1984.

[15]Middleton, W. D. and Lundry, J. L., "A System for Aerodynamic Design and Analysis of Supersonic Aircraft, Part I—General Description and Theoretical Development," NASA CR-3351, Dec. 1980.

[16]Lamar, J. E., "A Vortex-Lattice Method for the Mean Camber Shapes of Trimmed Noncoplanar Planforms with Minimum Vortex Drag," NASA TN D-8090, June 1976.

[17]Braslow, A. L. and Knox, E. C., "Simplified Method for Determination of Critical Height of Distributed Roughness Particles for Boundary-Layer Transition at Mach Numbers from 0 to 5.0," NACA TN-4363, 1958.

[18]Gingrich, P. B., Child, R. D., and Panageas, G. N., "Aerodynamic Configuration Development of the Highly Maneuverable Aircraft Technology Remotely Piloted Research Vehicle," NASA CR-143841, 1977.

[19]Aidala, P., "Numerical Aircraft Design Using 3-D Transonic Analysis With Optimization: User's Guide to Fighter Design Computer Program," AFWAL-TR-81-3091, Vol. III, Pt. 2, Aug. 1981. (Available from DTIC as AD A110037.)

[20]Mann, M. J., "The Design of Supercritical Wings by the Use of Three-Dimensional Transonic Theory," NASA TP 1400, Feb. 1979.

[21]Mann, M. J., Campbell, R. L., and Ferris, J. C., "Aerodynamic Design for Improved Maneuverability by Use of Three-Dimensional Transonic Theory," AIAA Paper 83-1859, July 1983.

[22]Takanashi, S., "An Iterative Procedure for Three-Dimensional Transonic Wing Design by the Integral Equation Method," AIAA Paper 84-2155, Aug. 1984.

[23]Cosentino, G. B. and Holst, T. L., "Numerical Optimization Design of Advanced Transonic Wing Configurations," AIAA Paper 85-0424, Jan. 1985.

[24]Davis, W. H. Jr., Aidala, P. V., and Mason, W. H., "A Study to Develop Improved Methods for the Design of Transonic Fighter Wings by the Use of Numerical Optimization," NASA CR, to be published.

[25]Schlichting, H., *Boundary Layer Theory,* 4th ed, McGraw-Hill Book Co., New York, 1962, p. 541.

[26]Sommer, S. C. and Short, B. J., "Free-Flight Measurements of Turbulent Boundary-Layer Skin Friction in the Presence of Severe Aerodynamic Heating at Mach Numbers from 2.8 to 7.0," NACA TN-3391, 1955.

[27]Hoerner, S. F., *Fluid Dynamic Drag,* published by the author, © 1965, pp. 6-6—6-17.